Time-Resolved X-Ray Spectral Studies of Laser-Compressed Targets*

D. T. Attwood, L. W. Coleman, J. T. Larsen, and E. K. Storm
University of California, Lawrence Livermore Laboratory, Livermore, California 94550
(Received 12 April 1976)

We present temporally and spectrally resolved x-ray emission data from a laser-irradiated target. The temporal dependence is interpreted in terms of a laser heating phase, a plateau period in which the glass-shell pusher propagates radially inward, a secondary x-ray burst corresponding to stagnation of the pusher at the target center, and a rapid decay of emission in the post-compression target disassembly period.

Experiments designed to confirm the concepts of laser-induced fusion[1] are under way in a number of laboratories. The essential features of this process, which is to be studied in these experiments, is the compression and heating of matter to thermonuclear conditions.[2,3] Typical experiments involve the irradiation of an approximately 100-μm-diam glass shell by an approximately 100-psec, terawatt neodymium-laser pulse. In contrast to the isentropic, ablatively driven implosions discussed in Ref. 1, these preliminary experiments are of an "exploding pusher" nature which, by comparison, are hydrodynamically more stable but result in less than optimal compressions.[4-6] Because of the high densities and temperatures expected, an important part of these experiments is the observation of temporally, spatially, and spectrally resolved x-ray emissions. Such observations can provide measures of significant physical parameters of the implosion process. We report in this paper the first observation of multichannel, spectrally resolved emission with sufficient temporal resolution to display the x-ray signal characteristic of the heating and implosion processes. Specifically, x-ray emission bands centered at 2.6, 4.0, and 5.3 keV, temporally resolved to 15 psec, show an overall emission envelope of 300 psec [for a 70-psec full width at half-maximum (FWHM) neodymium-laser pulse] characterized by a significant x-ray burst in the last 100 psec which we correlate with target compression. From these recorded x-ray temporal signatures we infer an implosion time of 180 psec and, consequently, an average implosion velocity of 2×10^7 cm/sec.

The JANUS laser-target irradiation facility, which is described elsewhere,[7] consists basically of a Nd-doped yttrium-aluminum-garnet oscillator with mixed yttrium-aluminum-garnet and glass amplifiers, culminating in a two-beam nominal 0.5 TW output at 1.064 μm. Two-sided target illumination is accomplished with a pair of $f/1$ aspheric lenses. In the experiment described here, an 87-μm-diam, 0.7-μm-wall-thickness glass microshell target was filled with a deuterium-tritium mixture to an initial density of 3 mg/cm^3. Upon simultaneous, two-sided irradiation by 70-psec (FWHM) pulses of 14.5 and 13.8 J, the target compressed and produced 4.6×10^6 neutrons. Time-integrated x-ray microscope photographs[8] indicate a change in radius of the compressed target by a factor of approximately 6. X-ray emission was detected with an ultrafast x-ray streak camera,[9] which is shown in a somewhat simplified manner in Fig. 1. X rays from the laser-irradiated target strike a slit-shaped gold photocathode causing the emission of electrons. This "slit" of electrons is then accelerated, deflected, and imaged onto a phosphor screen. By the application of a properly timed, strong ramp voltage, the slit image is swept quickly across the phosphor surface. Fast sweep speeds and small photoelectron velocity dispersion provide a 15-psec temporal resolution with this instrument. This value of time resolution is based on a measured photoelectron energy distribution for this photocathode,[10] and is consistent with both measured signal rise time presented herein

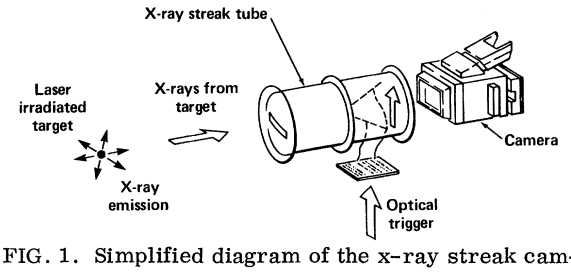

FIG. 1. Simplified diagram of the x-ray streak camera. An optical image intensifier, located between the streak-tube output phosphor and the recording camera, is omitted for clarity. The 100-Å gold photocathode is sensitive to x rays in the 1–10-keV range. The low-energy cutoff is determined by the 8-μm beryllium substrate.

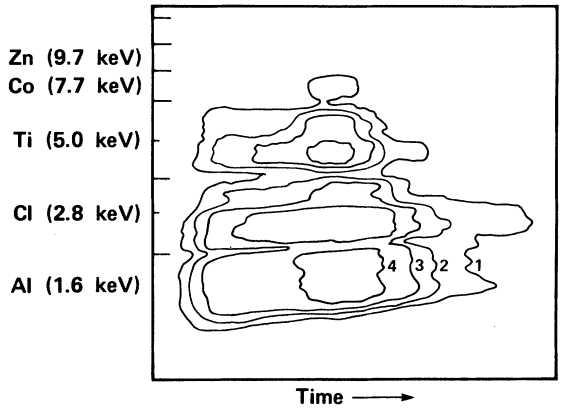

FIG. 2. Streak-camera photographic density contours showing temporal emission as a function of time for various K-edge filters. Numbers 1 through 4 refer to film density. Energies in parentheses refer to respective K-edge values.

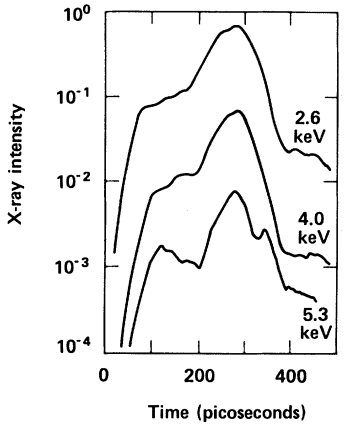

FIG. 3. Time-resolved x-ray emission from an 87-μm glass microshell irradiated from two sides with a total of 28 J in 70 psec. Quoted energies are mean values for the chlorine, titanium, and cobalt channels. Spectral widths are 0.3, 1.7, and 2.2 keV, respectively. The aluminum channel is not presented because of both film saturation and nonlocalized spectral contributions. The zinc channel showed no detectable emission in this particular experiment.

and resolution studies reported in the literature for similar instruments.[11,12] The image intensifier, used with the ultrafast streak camera to bring the data to a photographable level, is omitted in Fig. 1 for simplicity of presentation.

In order to record spectrally resolved x-ray emission from laser-irradiated targets, we employ a set of simple K-edge absorbers which cover the slit photocathode. X-ray filtering materials of aluminum, chlorine, titanium, cobalt, and zinc are used. Except for chlorine, the filters consist of high-purity metal foils, typically 25 μm thick. The chlorine filter consisted of commercially available polyvinylchloride (PVC). Double channels, of varying thickness, were used with the chlorine and titanium channels to provide exposure latitude and to check camera linearity in given spectral regions. The spectral region sampled by the chlorine K-edge filter is centered at 2.6 keV, with a 300 eV FWHM. This response is obtained by folding the foil transmission characteristic with the photocathode response and with the steeply falling x-ray emission spectrum that is measured by independent means.[13] The higher-energy channels are constructed to sample wider spectral regions and thus compensate for the dual problems of rapidly declining emission spectrum and photocathode response.

Figure 2 shows the streak-record photographic density contours obtained from the temporally and spectrally (but not spatially) resolved x-ray emission detected upon irradiation of the above described target. From this data profiles of film density versus time are obtained for each channel. Characteristics of the recording film are then removed with a simple computer program, thus converting the data to x-ray intensity versus time, on a channel-by-channel basis. Using recently measured[14] yield data for the gold photocathode, these channels can then be quantitatively related to one another in relative intensity, giving the time-resolved spectral data shown in Fig. 3. Time integration of these temporal profiles gives an emission spectrum that is in good agreement with that determined by the now standard time-integrated p-i-n diode measurements for this same target irradiation experiment.[13,15]

The measured x-ray temporal profiles presented in Fig. 3 are readily identified with general features of the exploding pusher process, pertinent aspects of which we briefly review here. In this process laser energy is absorbed in the plasma atmosphere and, by electron conduction, is rapidly transported throughout the glass pusher before significant hydrodynamic expansion takes place. According to numerical simulations of this process with the computer code LASNEX,[16,17] this results in a rapid heating of the glass pusher to an isothermal electron temperature of several hundred electron volts. During this heating phase there is a rapid rise in kilovolt x-ray emission from the shell region, reaching a crest approximately coincident with peak laser power. Now at

high temperature and pressure, the shell explodes both outwardly and inwardly, rapidly accelerating to a velocity of about 1×10^7 cm/sec in a few tens of picoseconds. The numerical calculations indicate that during the period beyond peak laser power, heating and acceleration play a diminishing role, resulting in a temporal plateau in kilovolt x-ray emission and a maximum shell velocity of about 3×10^7 cm/sec just before stagnation near the target center. At stagnation, kinetic energy of the pusher is converted to internal energy of both the shell and the enclosed DT gas, resulting in a secondary rise in x-ray emission. The calculations indicate a peak DT ion temperature of about 2 keV, resulting in a short burst of neutrons. However, the stagnated glass shell remains at an electron temperature of about 600 eV for several tens of picoseconds, continuing to radiate until extinguished by hydrodynamic expansion and radiative losses.

These general features of kilovolt x-ray temporal emission from an exploding pusher are all evident in the experimentally determined profiles of Fig. 3. In all three x-ray channels one observes the rapid rise in emission associated with shell heating, the plateau region in which laser heating and acceleration play a diminishing role, the secondary peak which corresponds to stagnation, and the final decay which accompanies post-compression target disassembly. A significant spectral feature observed in Fig. 3 is the relatively rapid decay of emission in the highest-energy x-ray channel (cobalt, 5.3 keV mean energy) between the first crest and the final peak. We interpret this spectrally sensitive data as experimental evidence of target cooling during the period extending from peak laser power to final stagnation. The average pusher velocity, a significant parameter in implosion studies, can be determined directly from the data presented here. According to the model described, the implosion time extends from the first crest in the emission history to the second peak, corresponding to stagnation. From the 4.0-keV channel of Fig. 3, the implosion time for this experiment is 180 psec. With initial and final radii of 43.5 and 7 μm, respectively,[8] the average pusher velocity is determined, within the accuracy of the model, to be 2×10^7 cm/sec, a value which agrees very well with the computed value.

In summary, we have measured temporally and spectrally resolved x-ray emissions which display temporal profiles consistent with a numerical simulation of laser-driven implosion of a glass microshell. Further x-ray streak-camera studies, including x-ray spatial imaging, are currently under way. The latter will permit us to observe separately temporal emission of x rays in the core and corona regions, further clarifying the data reported here.

The authors wish to acknowledge the contributions of several colleagues, particularly H. N. Kornblum, H. J. Weaver, G. Tripp, and members of the JANUS laser staff.

---

*Work performed under the auspices of the U. S. Energy Research and Development Administration, Contract No. W-7405-Eng-48.

[1]J. Nuckolls, L. Wood, A. Thiessen, and G. Zimmerman, Nature 239, 139 (1972).

[2]P. M. Campbell, G. Charatis, and G. R. Monty, Phys. Rev. Lett. 34, 74 (1975).

[3]V. W. Slivinsky, H. G. Ahlstrom, K. G. Tirsell, J. Larsen, S. Glaros, G. Zimmerman, and H. Shay, Phys. Rev. Lett. 35, 1083 (1975).

[4]G. H. Dahlbacka and J. Nuckolls, Bull. Am. Phys. Soc. 19, 950 (1974), and Lawrence Livermore Laboratory Report No. UCRL-75885 (unpublished).

[5]G. S. Fraley and R. J. Mason, Phys. Rev. Lett. 35, 520 (1975).

[6]J. F. Holzrichter, H. G. Ahlstrom, D. R. Speck, E. Storm, J. E. Swain, L. W. Coleman, C. D. Hendricks, H. N. Kornblum, F. D. Seward, V. W. Slivinsky, Y. L. Pan, G. B. Zimmerman, and J. H. Nuckolls, to be published.

[7]J. F. Holzrichter and D. R. Speck, J. Appl. Phys. 47, 2459 (1976).

[8]F. Seward, J. Dent, M. Boyle, L. Koppel, T. Harper, P. Stoering, and A. Toor, Rev. Sci. Instrum. 47, 464 (1976).

[9]C. F. McConaghy and L. W. Coleman, Appl. Phys. Lett. 25, 268 (1974).

[10]B. L. Henke, J. A. Smith, and D. T. Attwood, unpublished. In preliminary measurements with aluminum $K\alpha$ radiation (1487 eV) and a 100-Å gold photocathode, these authors find that the photoelectron energy distribution is dominated by slow secondaries with a peak at 1 eV and a nominal FWHM of 4 eV, depending somewhat on surface preparation.

[11]G. I. Brukhnevitch, V. K. Chevokin, Yu. S. Kasyanov, V. V. Korobkin, A. A. Malyutin, A. M. Prokhorov, M. C. Richardson, M. Ya. Schelev, and B. M. Stepanov, Phys. Lett. 51, 249 (1975).

[12]D. J. Bradley, A. G. Roddie, W. Sibbett, M. H. Key, M. J. Lamb, C. L. Lewis, and P. Sachsenmaier, Opt. Commun. 15, 231 (1975).

[13]V. W. Slivinsky, H. N. Kornblum, and H. D. Shay, J. Appl. Phys. 46, 1973 (1975).

[14]J. L. Gaines and R. A. Hansen, Lawrence Livermore Laboratory Report No. UCRL-77821 (unpublished).

[15]Agreement is within the nominal 25% unfold error associated with the wide-spectral-width filters em-

ployed here (see Fig. 3 caption), except that the 5.3-keV cobalt channel is 45% high for the streak camera. The relatively large error in this high-energy channel is likely related to the relatively weak recorded signal for cobalt, as observed in Fig. 2.

[16]J. T. Larsen, Bull. Am. Phys. Soc. 20, 1267 (1975), and Lawrence Livermore Laboratory Report No. UCRL-77040 (unpublished).

[17]G. B. Zimmerman, Lawrence Livermore Laboratory Report No. UCRL-74811, 1973 (unpublished).

Two-Dimensional Quasi-Linear Evolution of the Electron-Beam–Plasma Instability

K. Appert, T. M. Tran, and J. Vaclavik
Centre de Recherches en Physique des Plasmas, Ecole Polytechnique Fédérale de Lausanne, Switzerland
(Received 28 June 1976)

We report on the quasi-linear evolution of the electron-beam–plasma instability in a two-dimensional system. The numerical solutions of the basic equations show that a two-dimensional system evolves in a different way as compared with a one-dimensional system. After saturation the wave energy monotonically decreases with time while the width of its spectral distribution in k space narrows rapidly. In some cases, the system reaches a state which is modulationally unstable, and consequently cannot be described by the weak-turbulence theory.

In the problem of plasma heating, the turbulence excited by electron beams is of great importance. Various investigators have studied[1,2] the electron-beam–plasma interaction on the basis of the quasi-linear theory for the case when the turbulent oscillation spectrum is one-dimensional (wave vector $\vec{k}$ parallel to the motion of the beam). Such a model is appropriate when there is a magnetic field parallel to the beam in the plasma and when this field is strong enough to suppress oscillations that propagate at an angle to the beam axis. If there is a weak magnetic field in the plasma, so that $\omega_{pe} \gg \omega_{ce}$ (ω_{pe} and ω_{ce} are the plasma and the cyclotron frequencies of electrons, respectively), the turbulent spectrum becomes essentially three-dimensional. Such situations are met, e.g., in astrophysical problems or in the inertial confinement of plasmas. At present not much is yet known about the quasi-linear behavior of a three-dimensional turbulence excited by electron beams in a plasma. Attempts have been made to find at least certain general features of possible asymptotic states for the three-dimensional system.[3,4] However, these states seem to be too artificial and they have never been observed in experiments.[2] Thus the relaxation dynamics as well as the final state of the system remain unknown.

In this Letter we report on the two-dimensional quasi-linear evolution of the electron-beam–plasma instability. Since the problem exhibits axial symmetry with respect to the beam axis, the two-dimensional model is not restrictive[5] and was only chosen for convenience. The fundamental equations of the quasi-linear theory for the electron-beam–plasma interaction read[2]

$$\frac{\partial f}{\partial t} = \frac{\partial}{\partial \vec{v}} \cdot \pi \sum_{\vec{k}} \frac{\vec{k}\vec{k}}{k^2} I_{\vec{k}}\, \delta(\omega - \vec{k}\cdot\vec{v}) \cdot \frac{\partial f}{\partial \vec{v}}, \tag{1}$$

$$\frac{\partial I_{\vec{k}}}{\partial t} = \frac{2\pi I_{\vec{k}}}{k^2 \partial\epsilon/\partial\omega} \int d^2 v\, \vec{k} \circ \frac{\partial f}{\partial \vec{v}}\, \delta(\omega - \vec{k}\cdot\vec{v}), \tag{2}$$

where $\omega = 1 + 3k^2/2$, $\partial\epsilon/\partial\omega = 2 + 3k^2$, f is the velocity distribution function for electrons, and $I_{\vec{k}}$ is the spectral distribution of the electrostatic field associated with the oscillations. Equations (1) and (2) are in dimensionless units; the units of time, space, velocity distribution function, and spectral distribution are, respectively, ω_{pe}^{-1}, λ_D, $m_e n/T_e$, and $4\pi n T_e$. Here m_e, T_e, and n are the electron mass, temperature, and density, respectively, and λ_D is the Debye length.

We have solved Eqs. (1) and (2) by the finite-element method.[6,7] The algorithm consists of the following stages. First, Eq. (1) is put into the Galerkin (weak) form, the natural (Neumann) boundary condition being imposed on the velocity distribution function. The approximate solution for f is then assumed to be a combination $\sum f_i e_i$ of the linear pyramid basis functions $e_i(v)$. In this manner, Eqs. (1) and (2) are transformed into a system of ordinary differential equations in time for the quantities f_i and $I_{\vec{k}}$. This system of equations is solved numerically by an implicit, four-level, time-centered, finite-difference scheme.